Flame retardant potential of Tetra Pak®-derived biochar for ethylene-vinyl-acetate copolymers

Composites Part C: Open Access 8 (2022) 100252

Contents lists available at ScienceDirect

Composites Part C: Open Access

journal homepage: www.sciencedirect.com/journal/composites-part-c-open-access

Flame retardant potential of Tetra Pak®-derived biochar for ethylene-vinyl-acetate copolymers

Samuele Matta [a], Mattia Bartoli [b], Rossella Arrigo [a], Alberto Frache [a], Giulio Malucelli [a,*]

[a] Politecnico di Torino, Department of Applied Science and Technology and local INSTM Unit, Viale Teresa Michel 5, Alessandria 15121 Italy
[b] Center for Sustainable Future Technologies - CSFT@POLITO via Livorno 60, Torino, 10144 Italy

ARTICLE INFO

Keywords:
Biochar
Ethylene-vinyl-acetate copolymer
Flame retardant
Forced-combustion behavior
Mechanical properties

ABSTRACT

Food packaging waste-stream is a serious threat for current lifestyle sustainability. Among all the materials, Tetra Pak® is one of the most employed to produce food and beverage containers. Its composition represents a challenge for waste management due the simultaneous presence of poly(ethylene), paper and aluminum, wrapped together into a multilayered packaging. In this work, we report on the pyrolytic conversion of Tetra Pak® to produce alumina-rich biochar (BC), to be used as a flame retardant for an ethylene-vinyl-acetate (EVA) copolymer. In particular, the obtained biochar was incorporated either into bulk EVA through compounding or just as a surface coating. For the surface approach, a masterbatch of biochar and EVA was prepared and then applied to the surface of unfilled EVA specimens. Both the strategies turned out to significantly improve the overall flame retardant features of the copolymer: as compared to unfilled EVA, the bulk approach promoted a remarkable decrease of peak of heat release rate (-45 and -65%, for the compounds containing 20 and 40 wt.% of BC, respectively) and of total heat release (-16.9% for the compounds filled with 40 wt.% of BC), combined with a significant increase of the residues at the end of forced combustion tests; conversely, the surface approach was capable of delaying the time to ignition and the time to peak of heat release rate, depending of the BC amount: more specifically, for the surface-coated EVA with the lowest BC loading (i.e. 3 wt.%), the two parameters increased by about 34 and 21%, respectively. The thermal, rheological and mechanical properties were also investigated, as well as the morphology of the BC particles and their dispersion in the copolymer matrix. In particular, increasing the biochar loading promoted an increase of the stiffness of the resulting compounds, as well as a decrease of their ductility with respect to unfilled EVA.

1. Introduction

Recycling composites materials is a very intriguing challenge in the waste management field, due to the heterogeneity of the waste streams [1]. Among the multilayered packaging composites, Tetra Pak® [2] is the most used due to its mechanochemical resistance [3] and compatibility with a wide range of foods and beverages [4]. The disposal of Tetra Pak® is a challenging task due to the simultaneous presence of paper, aluminum foils and poly(ethylene). Since its first appearance on the market, the end-life destiny of Tetra Pak® has been the focus of a great attention from both industrial and academic research [5]. Several efforts have been made so far in order to valorize Tetra Pak® waste-streams, hence preventing their landfill confinement. In particular, Tetra Pak® waste-streams can be managed by re-use after grinding as filler for cementitious matrices [6, 7] and wood laminates [8], by separating the different constituents [9, 10] or through conversion processes. A possible Tetra Pak® waste-stream conversion route is represented by hydrolytic treatments for the recovery of cellulose nanocrystals from the paper layers, as reported in the literature [11, 12]. Nevertheless, this method requires a high cost for the isolation of the products and it is unable to efficiently taking care of poly(ethylene) and aluminum fractions. Conversely, pyrolysis represents a more robust solution for a sustainable disposal of Tetra Pak® with a high energy efficiency [13, 14] and the production of fuels and chemicals [15, 16].

Pyrolytic treatments of neat or mixed biomasses also lead to the formation of a solid residue that is commonly known as biochar (BC) [17]. BC is generally exploited at pre-industrial scale as soil amendment [18], though it has found many other applications ranging from environmental remediation [19] to advanced materials science for the production of new materials and composites [20–28]. A few works

* Corresponding author.
E-mail address: giulio.malucelli@polito.it (G. Malucelli).

https://doi.org/10.1016/j.jcomc.2022.100252
Received 21 December 2021; Received in revised form 23 February 2022; Accepted 3 March 2022
Available online 5 March 2022

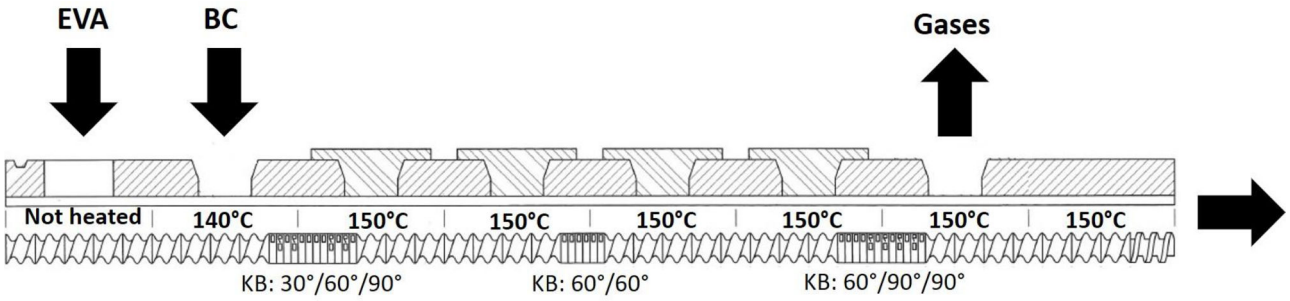

Fig. 1. screw and temperature profile of the instrument used during extrusion process (KB = kneading blocks).

demonstrated the possibility to obtain BC from the pyrolytic treatment of Tetra Pak® wastes, exploiting different reactors and processing conditions [29–31]. As an example, Ding et al [32]. investigated a two-step process, involving an acid pretreatment and a slow pyrolysis at 600 °C, to produce an aluminum-enriched BC with excellent sorption performance for arsenic, potentially suitable for wastewater treatment. Similarly, Zúñiga-Muro et al [33]. evaluated a pyrolytic process of Tetra Pak® for the preparation of BC employable as adsorbent for mercury removal from aqueous solutions. The authors proved that the pyrolysis conditions, such as temperature and treatment time, strongly affect the yields and the physico-chemical properties of the solid product, demonstrating the versatility of the exploited process in the Tetra Pak® wastes valorization.

Contrary to pure biomass derived BC, Tetra Pak®-derived BC is characterized by a high inorganic fraction due to the aluminum foils, which is unsuitable for soil uses but may represent an advantage for the production of composites with increased flame retardance [34–37].

The suitability of BC as a flame retardant, alone or in combination with other additives has been already reported in the scientific literature. In this regard, Das and co-workers prepared polypropylene-biochar composites using biochar derived from pine wood feedstock, which was pyrolyzed at 500 °C and successively activated at 900 °C. The biochar loading was varied between 15 and 35 wt.%. As assessed by forced-combustion tests, the presence of increasing amounts of filler turned out to significantly lower the peak of heat release rate with respect to the unfilled polymer (up to about −55% for the composite incorporating the highest filler loading) [33].

In a further research effort, Ikram et al [34]. proved that the incorporation of 36 wt.% of biochar into polypropylene was responsible for an improved thermal stability, as well as for a remarkable decrease of the peak of heat release rate (by about 50% as compared with the unfilled polyolefin).

Synergistic effects were then demonstrated when the same biochar was incorporated, together with wool fibers, into polypropylene, in the presence of 20 wt.% of ammonium polyphosphate, employed as an intumescent flame retardant. 25 wt.% of Biochar and 10 wt.% of wool fibers were enough to increase the limiting oxygen index (which was found as high as 23%, vs. 18% for unfilled polypropylene) and to lower the peak of heat release rate by about 70%, as compared with the neat polyolefin.

Further, the peak of heat release rate values of biochar-pine wood-polypropylene composites (total amount of fillers loading: 34 wt.%) were found to decrease by 60–65% in the presence of ammonium polyphosphate (at 20 wt.% loading), as compared with the unfilled polymer matrix [38]. Similar performances were obtained by replacing ammonium polyphosphate with magnesium hydroxide in the formulation of the composites, although their overall flame retardant behavior was somewhat lower as compared with ammonium phosphate-containing systems. In a general view, the highly thermally stable biochar accounted for the formation of a protective char layer, able to slow down the transfer of oxygen to the burning polymer and of the combustible gaseous products derived from the decomposition of the polyolefin to the surroundings [38–40] .

In this work, we report on the conversion of Tetra Pak® through pyrolytic process to produce a BC rich of alumina. The obtained product was employed as a flame retardant in EVA. More specifically, two different strategies were exploited: the first dealt with the incorporation of the filler into the bulk copolymer; the second utilized a pre-prepared BC-EVA masterbatch that was applied, as a surface coating, onto unfilled EVA specimens. This latter approach has been already proposed and discussed in the literature, showing its suitability and effectiveness in providing protection to an underlying polymer matrix. In fact, although flame retardants dispersed in the polymer bulk have clearly demonstrated to be efficient, nowadays there exist an increasing attention on the utilization of surface methods, capable to concentrate the flame retardant action on the surface of a polymer system, where combustion specifically takes place: consequently, the required features of the polymer bulk are preserved, and the quantity of flame retardant is minimized [41]. In a previous work [42], we compared the effectiveness of DNA as flame retardant for EVA copolymers, when dispersed in the polymer bulk or just directly deposited on the surface: being equal the deposited amount of biomacromolecule on the surface and dispersed into the bulk, the surface method turned out to be very effective in blocking the ignition of polymer, as assessed by forced-combustion tests carried out with an irradiative heat flux of 35 kW/m2, rising the time to ignition (+380% with respect to neat EVA), and significantly delaying it (+625% with respect to neat EVA) when the specimens were exposed to a higher irradiative heat flux (50 kW/m2). The bulk and surface approaches were also compared for protecting polyamide 10, 10 from fire [43]: n particular, a standard intumescent formulation, made of ammonium polyphosphate, ammonium polyphosphate and pentaerythritol or ammonium polyphosphate and starch, was either dispersed in the polymer bulk, or embedded in an UV-curable waterborne acrylic resin and applied as a surface coating. This latter approach, compared to the bulk method, was found to be very effective in lowering the peak of heat release rate (by about 65%), without significant differences in the total heat release decrease.

Therefore, in this work we discuss the effectiveness of the two approaches on the flame retardant features of the selected copolymer: The preliminary idea was to use the same amount of BC for preparing both the bulk and the surface-coated samples. However, for achieving 20 and 40 wt.%, the filler amount required for producing the masterbatches for the surface approach would not have allowed the processing in the extruder. Therefore, we decided to prepare masterbatches containing 3 and 6 wt.% of BC: despite the low filler loadings (much lower with respect to the amount of biochar embedded in the copolymer bulk), these two selected loadings were found capable to enhance the behavior in forced-combustion tests, providing a good protection to the underlying unfilled EVA.

2. Materials and methods

2.1. Materials

EVA (Greenflex MQ40, density: 0,942 g/cm^3; vinyl acetate content: 19 wt.%; melt flow rate: 12 g/10 min at 190 °C/2.16 kg), was provided by Versalis S.p.a., Mantova, Italy.

Tetra Pak® was collected from urban and domestic waste streams. It was washed and dried at 105 °C for 72 h prior pyrolytic conversion.

2.2. Production of BC

Tetra Pak® was chopped into squared pieces of around 3 × 3 cm. 100 g was pyrolyzed using a tubular furnace (Carbolite TZF 12/65/550) in nitrogen atmosphere, using a heating rate of 15 °C/min up to 800 °C for 30 min, as previously reported [43, 44]. After cooling down at room temperature, BC was recovered and mechanically pulverized using a mechanical blender for 10 min and operating at room temperature, prior to be used for the preparation of the compounds.

2.3. Preparation of compounds

A co-rotating twin-screw extruder Process 11 from ThermoFisher Scientific (Waltham, MA, USA) with 11 mm screw diameter and 40 L/D ratio, was employed for processing the compounds; the temperature profile of the screw is presented in Fig. 1. 500 rpm (extruder speed) and 350 g/h (mass flow of the copolymer) were set, following the conditions optimized in a previous work [34].

The pellets obtained from the extrusion process were processed for forced-combustion tests as square samples (100 × 100 × 3 mm^3), using a Collin P200T press (Maitenbeth, Germany), equipped with hot plates for compression molding and operating at 150 °C and 100 bar for either unfilled EVA or its compounds in bulk at 20 and 40 wt.% (coded as 20BC-T and 40BC-T, respectively). The same conditions were adopted to mold 500 μm thick layers of EVA-BC (BC loading: 3 and 6 wt.%), which were subsequently welded to the neat EVA square samples (operating at 80 °C and 100 bar). The resulting welded specimens were coded as 3 BCE-T-up and 6 BCE-T-up, depending on the BC loading in the thick surface layer.

Further, a Babyplast 610P Standard injection molding machine, purchased from CRONOPLAST SL (Abrera, Spanish) was employed for obtaining dog bone shaped specimens for the mechanical tests [34].

2.4. Characterization techniques

Raman spectra were collected by using Renishaw® Ramanscope InVia (H43662 model, Gloucestershire, UK). Signals were fitted according to methodology proposed by Tagliaferro et al [44]..

The ash content was evaluated by putting 1 g of BC into an alumina crucible, heating it in air with a heating rate of 10 °C/min up to 800 °C and keeping it at this temperature for 1 h. Three tests were performed, and the results averaged.

The BC surface was investigated by using X-ray photoelectron spectroscopy (XPS). To this aim, a PHI 5000 Versaprobe Physical Electronics (Chanhassen, MN, USA) scanning X-ray photoelectron spectrometer (monochromatic Al K-alpha X-ray source with 1486.6 eV energy, 15 kV voltage, and 1 mA anode current) was employed for evaluating the surface chemical composition.

Specific surface area of the samples was measured by means of N_2 sorption at −196 °C on a micrometrics Tristar II instrument (Micromeritics Instrument Corporation, USA). The Brunauer–Emmett–Teller (BET) model was applied.

An EVO 15 scanning electron microscope (SEM) from Zeiss (Oberkochen, Germany), coupled with Ultim Max 40 energy dispersive X-ray (EDX) micro-analyzer by Oxford Instruments (High Wycombe, UK) was utilized for assessing the morphologies of EVA/BC composites; the samples, fractured in liquid nitrogen, were fastened to a conductive adhesive tape and gold metallized.

Rheological measurements were performed using an ARES (TA Instrument, New Castle, DE, USA) strain-controlled rheometer, employing a parallel plate geometry (plate diameter: 25 mm; gap between the plates: 1 mm). The complex viscosity values were measured through frequency scans ranging from 10^{-1} to 10^2 rad/s at constant temperature (150 °C). The strain amplitude was chosen for each sample in order to fall in the linear viscoelastic region.

Differential scanning calorimetry (DSC) tests were carried out on a Q20 TA Instrument apparatus (New Castle, Delaware USA), using sealed aluminum pans and operating in dry nitrogen. The following thermal cycle was followed:

- heating up from 30 to 150 °C at 10 °C/min
- cooling down from 150 °C down to 30 °C at 10 °C/min
- heating up from 30 to 150 °C at 10 °C/min

The second heating up was exploited for measuring melting and crystallization temperatures (T_m and T_c, respectively), as well as melting (ΔH_m) and crystallization (ΔH_c) enthalpies. X_c, i.e. the crystallinity degree of all the investigated systems, was calculated as follows:

$$X_c = \frac{\Delta H_m}{\Delta H_{100}\ (1-x)} * 100$$

where ΔH_{100} is the melting enthalpy of the 100% crystalline polymer matrix (referred to polyethylene segments only) and x represents the wt. % of BC.

The thermal and thermo-oxidative behavior of BC powders and EVA-BC composites was assessed through (TG) thermogravimetric analyses: to this aim, a Q500 system from TA Instrument (New Castle, Delaware, USA) was employed. Around 10 mg of each sample was placed into an open alumina crucible and heated up from room temperature to 800 °C (heating rate: 10 °C/min), either in 60 ml/min air or nitrogen gas flow. The following parameters were measured: T_{onset} (temperature, at which the sample starts degrading), T_{max} (temperature of the peak of dTG - derivative - curves) and residues at the related temperatures, as well as at the end of the tests.

Cone calorimetry tests were carried out with a Fire Testing Technology (West Sussex, UK) instrument, following the ISO 5660 standard. Each sample (size: 50 × 50 × 3 mm^3) was tested under a 35 kW/m^2 irradiative heat flux in horizontal configuration. The following parameters were evaluated: peak of heat release rate (pHRR, kW m^{-2}), time to peak (s), total heat release (THR, kW m^{-2}), Time to ignition (TTI, s), fire performance index (FPI, (kW m^{-2}) s^{-1}), fire growth rate index (FIGRA, (kW m^{-2}) s^{-1}), total smoke release (TSR, m^2 m^{-2}), specific extinction area (SEA, m^2 kg^{-1}), and the residues at the end of the tests.

Finally, the Flame Retardancy Index (FRI), a dimensionless parameter defined by the following equation

$$FRI = \frac{\left[THR * \left(\frac{pHRR}{TTI}\right)_{unfilled\ EVA}\right]}{\left[THR * \left(\frac{pHRR}{TTI}\right)_{EVA-BC\ compound}\right]}$$

was calculated [45] it allows comparing the flame retardant performances of thermoplastics irrespective of the type of polymer and flame retardants employed.

The temperatures involved during combustion were recorded using a K-type thermocouple (diameter of 1 mm) from Tersid (Milan, Italy) and a K-type thermocouple integrated on a heat resistant plate (size: 100 × 100 mm^2) from Thermo Electra (Pijnacker, Netherlands). The first thermocouple was placed in contact with the sample surface exposed to the cone heater, in the middle of the sample, for collecting the temperature on the top; the second one was used as a support for the specimen, in order to collect the bottom temperature. Specimens of 100 × 100 × 3 mm^3 were used; the tests were repeated at least three times

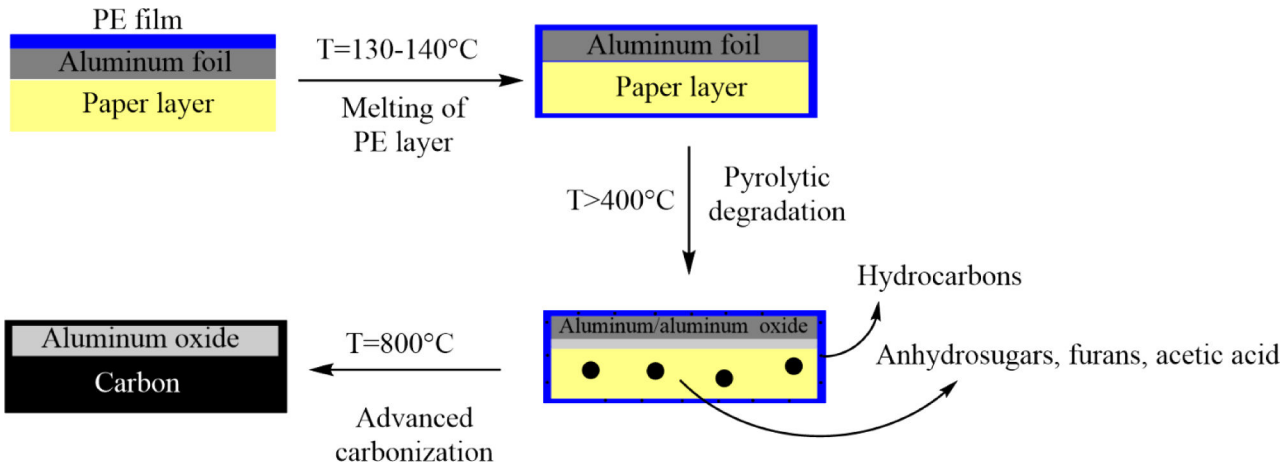

Fig. 2. Schematic pathway of Tetra Pak® pyrolysis for BC production.

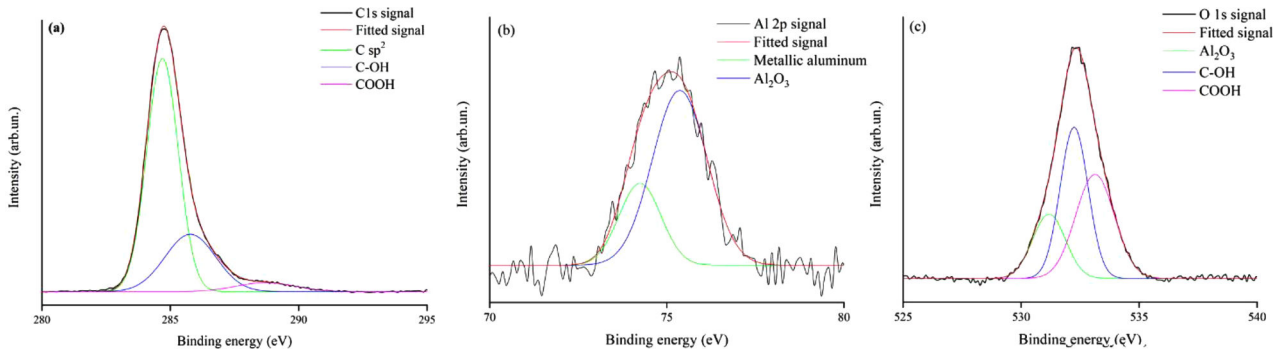

Fig. 3. XPS spectra of a) carbon, b) aluminum and c) oxygen of BC.

and the results averaged.

An Instron 5966 dynamometer (Norwood, MA, USA) was employed for assessing the mechanical behavior through tensile tests, according to the ISO 527 standard. A 5 kN load cell was utilized, working at 1 mm/min rate until 0.2% deformation was achieved; afterward, the rate was boosted up to 50 mm/min till the specimen fracture. Five specimens were tested for each system and the results (in terms of tensile modulus (E) and the elongation at break (ε)) averaged.

3. Results and discussion

3.1. BCE characterization

The pyrolysis of waste multilayers packaging takes place through a series of different steps schematized in Fig. 2.

In the very early stage, poly(ethylene) layers undergo a melting process, providing an homogeneous environment for the subsequent thermal cracking reactions that take place beyond 400 °C. In this latter condition, cellulose degradation occurs with the release of anhydrosugars and furans that undergo further degradative processes, leading to a massive production of acetic acid [46]. This latter can be boosted up by the addition of inorganic oxides [47] and metals such as the aluminum foil present in the Tetra Pak® multilayer. The high temperatures, together with the acidic atmosphere, could induce an extensive oxidation of the aluminum layer with the formation of alumina as clearly emerged from the XPS analysis reported in Fig. 3.

As clearly shown in Fig. 3b, alumina (Al 2p 75.4 eV) represents the greatest part of aluminum species, reaching 74% of abundance; its presence can also be appreciated from the O1s component peaked at 531.1 eV. The presence of other aluminum compounds can be excluded due to the instability of such species as $Al_2(CO_3)_3$ [48] and the absence of peaks attributable to AlOOH or $Al(OH)_3$ [49]. BC carbon components show the absence of sp^3 species with the massive presence of sp^2 carbon (284.7 eV) tailored with hydroxyl (C1s 285.8 eV, O2p 532.1 eV) and carboxylic (C1s 289.2 eV, O2p 533.2 eV) functionalities. The considerable presence of sp^2 carbon has led to a quite ordered carbonaceous materials as shown in Fig. 4. Compared with systematic studies reported by Tagliaferro et al [44]., BC shows a sharper D and G peaks with respect to the BC produced in temperature range within 700 and 1000 °C, with a partially structured 2D region and with an I_D/I_G ratio of 1.1. This finding can be attributed to the advanced carbonization promoted by the synergistic effect of homogenous pyrolytic environment provided by the poly(ethylene) melted together with the aluminum species.

The unique features of Tetra Pak® derived BC can be also appreciated by the FESEM pictures shown in Fig. 5.

BC shows a morphology consisting of sub-micrometric carbon particles clustered into structures within 1 and 10 mm and a surface area of up to 42.4 m2/g. Interestingly, the big particle aggregates consist of micrometric and submicrometric particles with an average radius of 1.2 ± 0.2 mm. Remarkably, aluminum-rich flakes are quite uniformly dispersed as shown in Fig. 5a. Nevertheless, at a sub-micrometric scale some differences are appreciable as shown by EDX analysis (table 1) carried out in the regions 1 and 2 of Fig. 5a. Finally, it is worthy to note that BC also contains Calcium and Silicon, which can be attributed to the paper layer of Tetra Pak®, as these elements are commonly present during the paper manufacturing [50]. Compared with the aluminum content of virgin Tetra pak® (about 5 wt.% as reported by the producer), BC showed a higher ash content (namely, 11.3 ± 0.9 wt.%) mainly due to the presence of aluminum residues.

EDX analysis clearly shows a different composition between regions

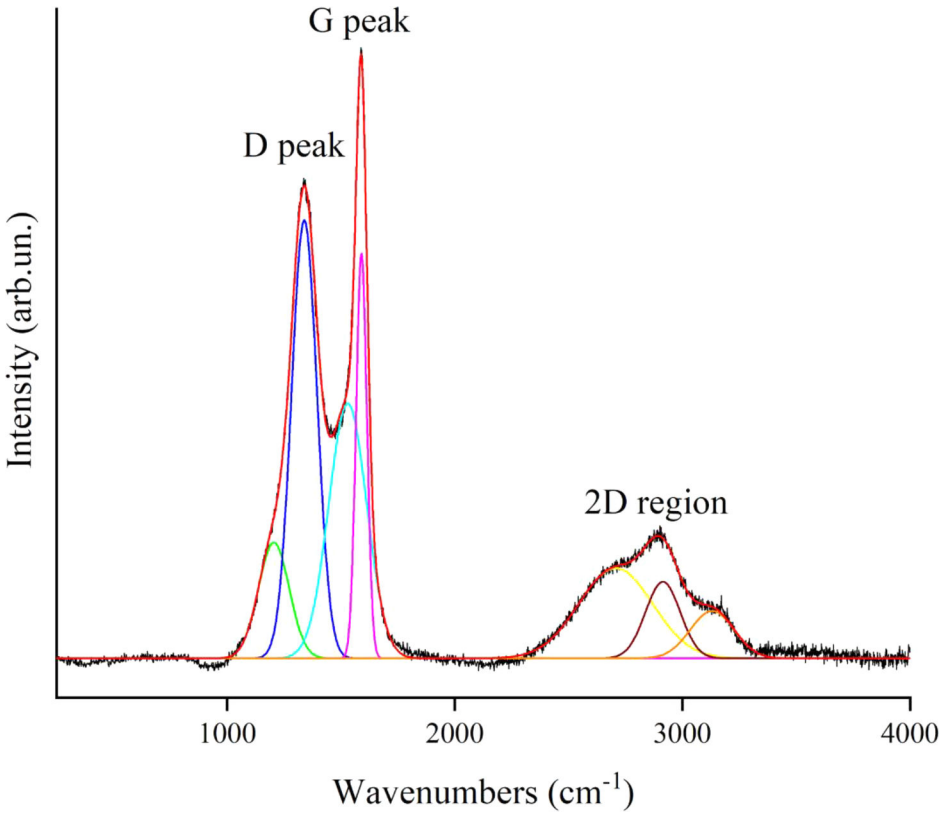

Fig. 4. Raman spectra of BC in the range from 500 cm−1 up to 4000 cm−1.

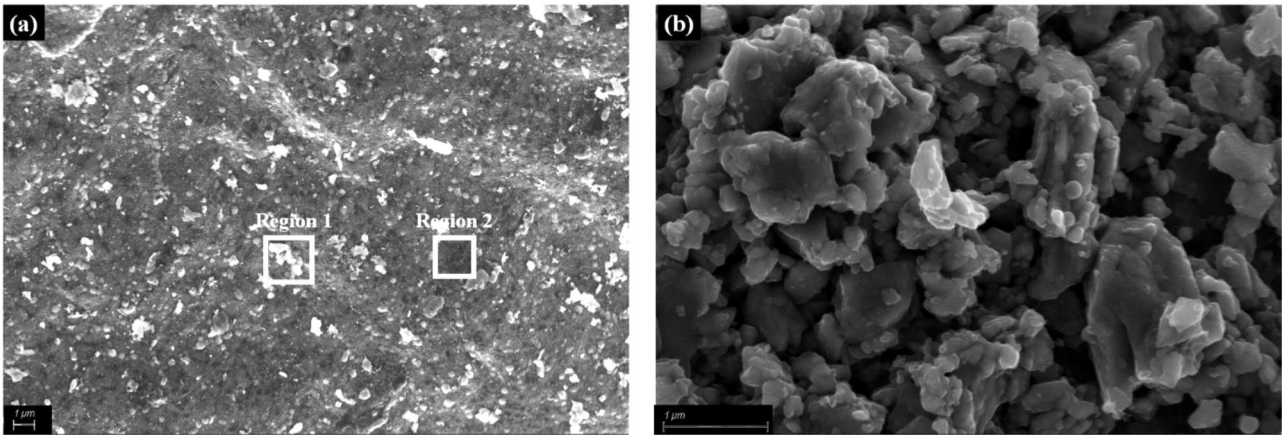

Fig. 5. FESEM capture of BC with magnification of a) 0.5 K and b) 20 K. Aluminum- (region 1) and carbon-rich (region 2) regions are highlighted in white.

Table 1
Elemental composition obtained through EDX analysis of region 1 and region 2 of BC.

Element	Weight(%)	
	Region 1	*Region 2*
Carbon	24.5	60.4
Oxygen	22.3	27.9
Aluminum	51.4	0.5
Silicon	0.2	1.3
Calcium	0.2	8.8
Sodium	1.3	1.1

1 and 2. The carbon-rich region (region 2) is characterized by a negligible amount of aluminum (not exceeding 0.5 wt.%), which, conversely, reaches 51.6 wt.% in region 1. Noticeably, the aluminum-rich region shows a carbon content up to 24 wt.%, which supports the hypothesis that even in this case a carbon layer is mixed with the aluminum flakes, though it is not possible to argue on the uniformity of carbon layer onto aluminum flakes.

Table 2
tensile properties of EVA and its compounds.

Sample	Tensile modulus (E) [MPa]	Elongation at break (ε)[%]
EVA	50 ± 2	123 ± 6
20 BCE-T	117 ± 6	90 ± 10
40 BCE-T	246 ± 34	31 ± 7

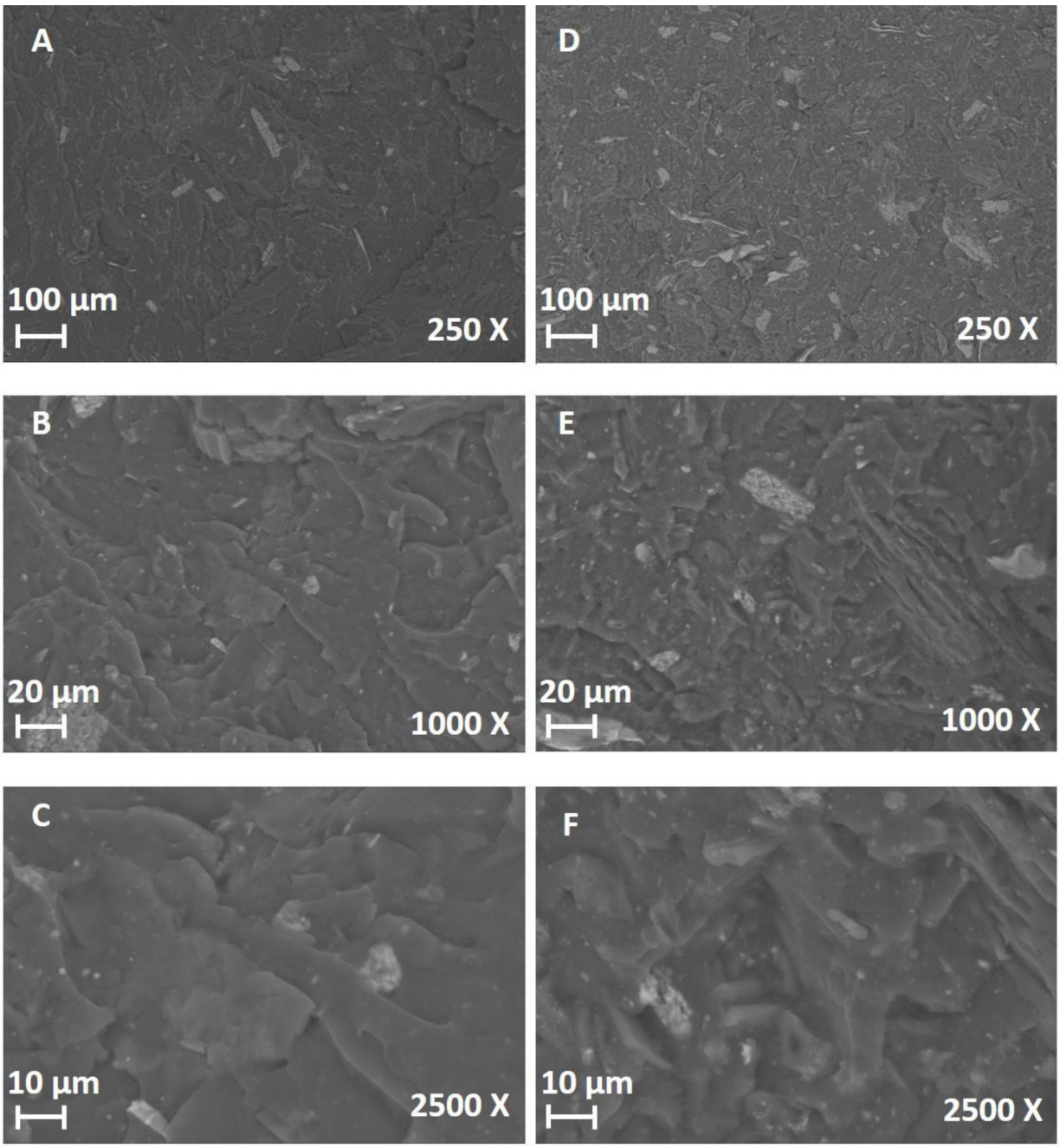

Fig. 6. SEM images at different magnification of the bulk compounds containing 20 wt.% (A, B, C) and 40 wt.% (D, E, F) of BC.

3.2. Mechanical behavior

Tensile tests were carried out on EVA and its bulk compounds, in order to assess the effect of the presence of the BC on the overall mechanical behavior of the copolymer Table 2. collects the results in terms of tensile modulus and elongation at break. As expected, the incorporation of BC increases the stiffness: in particular, the tensile modulus monotonically increases when the BC loading increases, achieving 246 MPa for the compound containing 40 wt.% of BC, i.e. more than four times higher than that of unfilled EVA ($E = 50$ MPa). Conversely, the ductility of EVA copolymer is remarkably worsened in the presence of the filler. These results are in agreement with the behavior of EVA filled with its traditional flame retardants (i.e. hydroxides, hydroxycarbonate, ammonium polyphosphate, aluminum trihydrate), as nicely reported in literature [51, 52].

Therefore, the proposed flame retardant strategy of incorporating BC into the copolymer bulk, though being effective as far as the overall fire behavior is concerned, is, on the other hand, responsible for an important toughness loss, which has to be taken into account when the flame retarded copolymer has to withstand specific mechanical stresses, depending on the final application.

3.3. SEM-EDX analyses on the compounds and on the coated EVA

SEM observations were performed on EVA-BC compounds in order to investigate the morphology of the filler as well as its distribution within EVA. Furthermore, EDX micro-analyses were performed on the compounds in order to further confirm the degree of dispersion of the filler in the copolymer matrix.

Fig. 6 shows some typical SEM images at different magnifications of

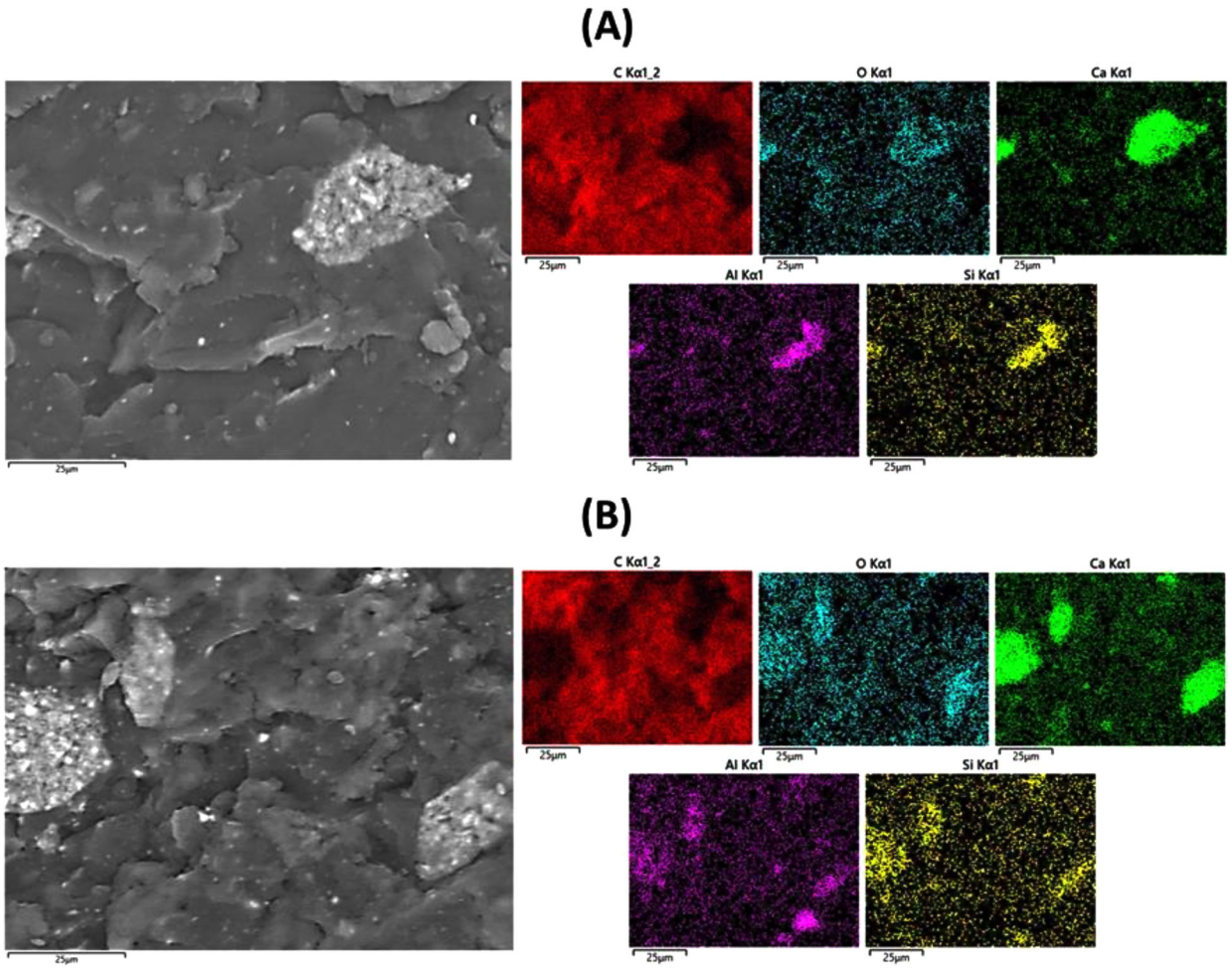

Fig. 7. EDX maps of the elements included in biochar for the bulk compounds containing 20 wt.% (A) and 40 wt.% (B) of BC.

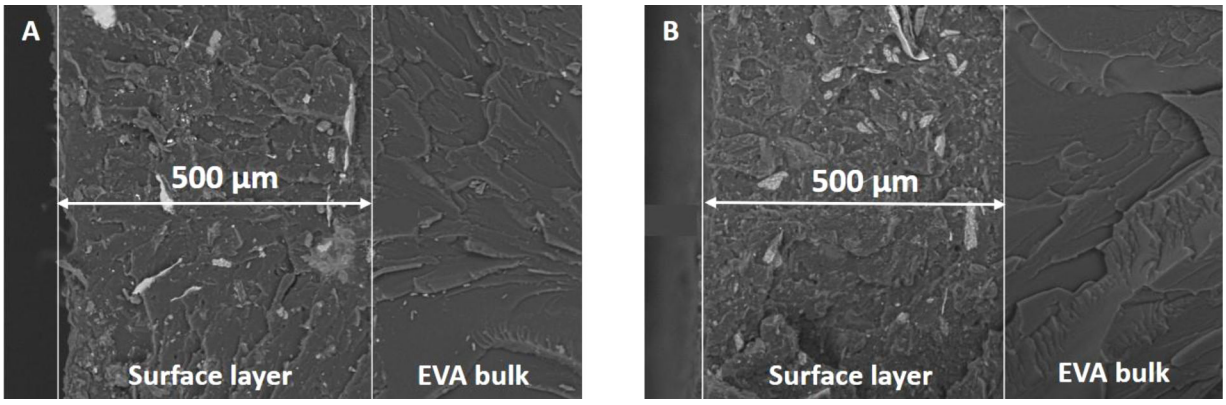

Fig. 8. EVA coated with EVA layers containing 3 wt.% (A) and 6 wt.% (B) of BC.

the compounds containing 20 and 40 wt.% of BC. Particles are well distributed within the polymer matrix and their size is substantially micrometric and submicrometric, according to the average size of BC; besides, some bigger aggregates (not exceeding 100 µm) are clearly visible. These findings indicate that the experimental conditions adopted for compounding were suitable for obtaining a quite homogeneous dispersion of the filler within EVA. The good distribution of BC within the copolymer matrix is further supported by the EDX maps of the main elements contained by BC (Fig. 7).

Finally, SEM analyses were performed also on the cross-sections of the samples coated with the BC-rich film. The thickness of the coatings (at 3 and 6 wt.% of BC) is independent from the filler loading and is about 500 µm; the separation from the underlying EVA is clearly visible in Fig. 8. Furthermore, these images clearly indicate a homogeneous distribution of the filler in the surface coating, despite the presence of some aggregates, the size of which does not exceed 100 µm.

3.4. Rheological analyses

Fig. 9 shows the complex viscosity curves of unfilled EVA and its

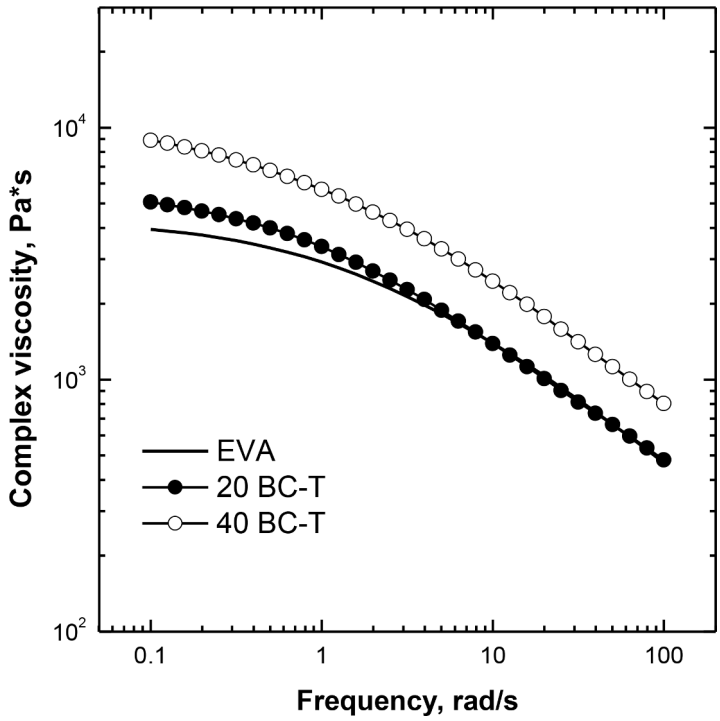

Fig. 9. Complex viscosity curves for EVA and BC-containing composites.

Table 3
results from DSC analyses for EVA and its compounds with BC.

Sample	T_c (°C)	ΔH_c (J/g)	T_m (°C)	ΔH_m (°C)	Xc (%)
EVA	62.7	27.6	85.3	13.2	4.5
20 BCE-T	64.6	22.3	85.4	7.2	3.1
40 BCE-T	64.9	11.9	85.0	5.3	3.0

compounds with BC. The neat matrix exhibits the typical viscosity trend of unfilled polymeric materials, i.e. a Newtonian behavior in the low frequency range, followed by the shear-thinning region, involving a rapid decrease of the complex viscosity values as a function of frequency. The introduction of 20 wt.% of BC induces a slight enhancement of the complex viscosity values as compared to the unfilled matrix in the low frequency range, without significantly modifying the material rheological response at high frequencies. The further increase of the BC loading causes the obtainment of higher complex viscosity values in the whole investigated frequency range, though the frequency-dependence of the viscosity curve of the composite containing 40 wt.% of BC remains quite similar to that of the unfilled matrix. The obtained results suggest a moderate effect of the embedded filler on the relaxation dynamics of EVA macromolecules, according to similar results reported in literature for composites containing micrometric BC particles27, and the rheological behavior of the composite materials is mainly governed by the viscoelastic response of the matrix macromolecules.

3.5. DSC analyses

The main DSC data gathered during the selected thermal cycle for EVA and its compounds are presented in Table 3. The thermogram of EVA shows a typical melting peak at 85.3 °C and the crystallization process occurs at 62.7 °C. It is worthy to note that the presence of BC, irrespective of its loading, does not affect the melting temperature of the compounds, which is almost the same of unfilled EVA (about 85 °C). Besides, Tc is substantially unaffected by the presence of the filler, as it slightly increases by about 2 °C, regardless of the filler loading.

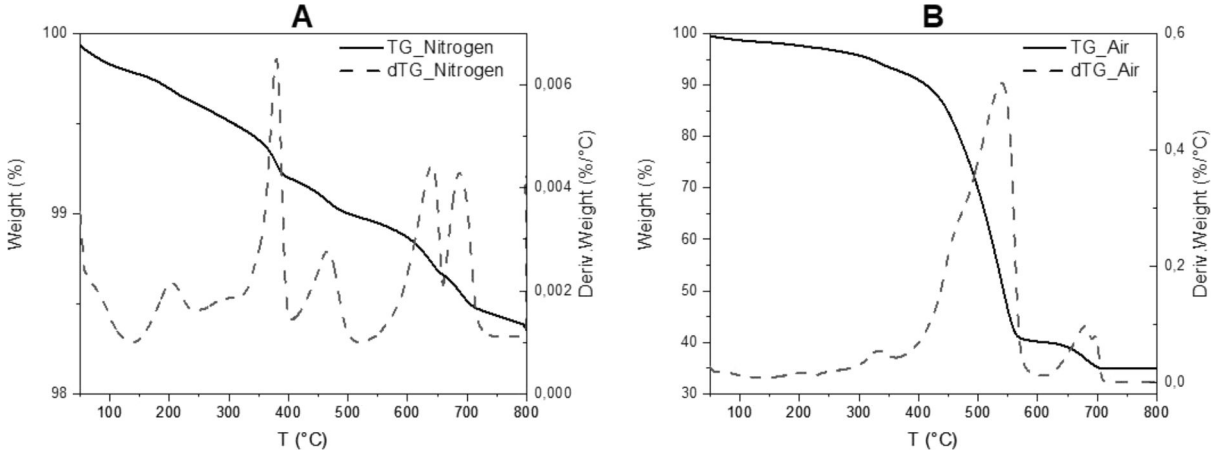

Fig. 10. TG and dTG curves of BC in nitrogen (A) and in air (B).

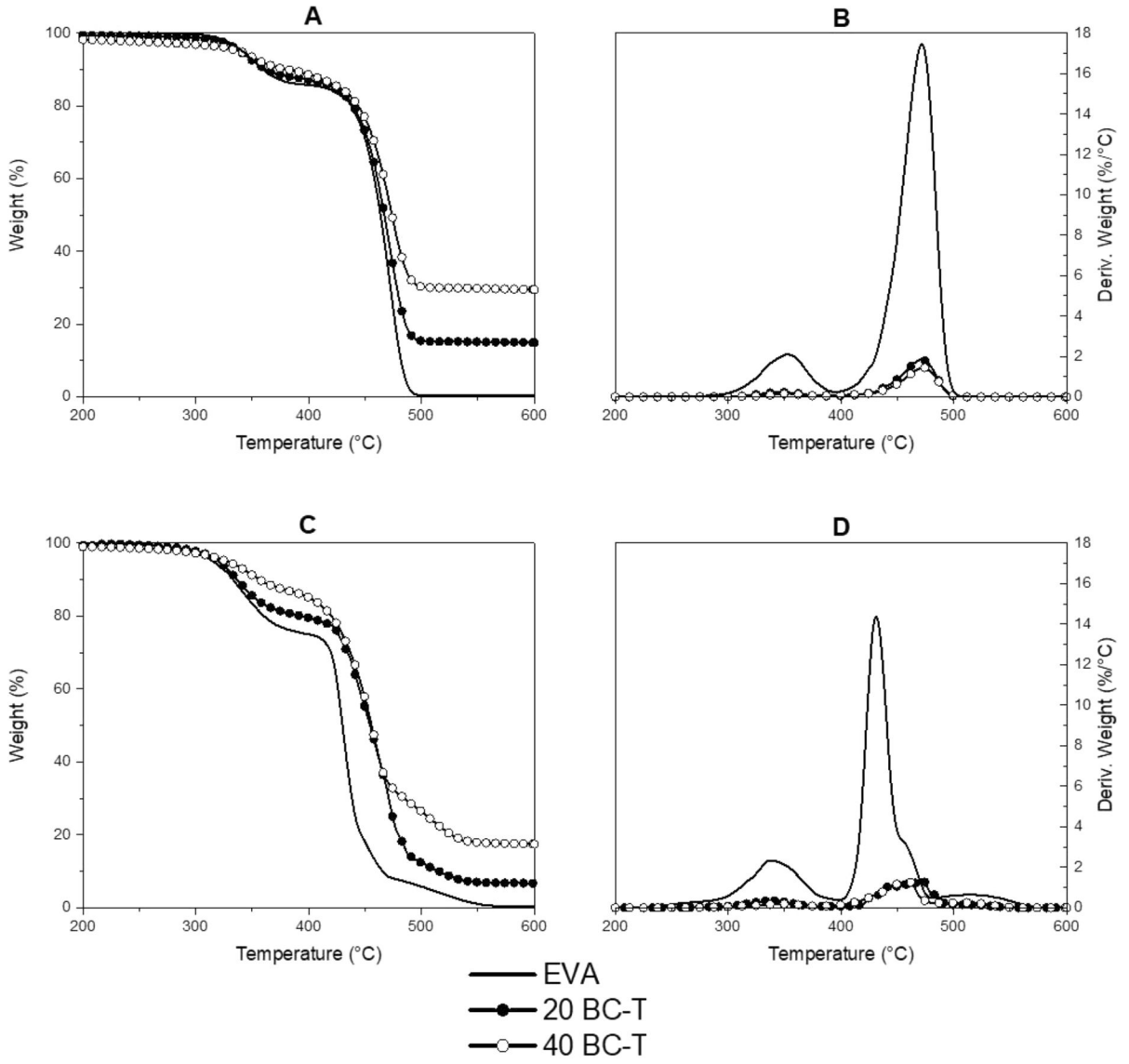

Fig. 11. TG and dTG curves of EVA and its compounds in nitrogen (A,B) and in air (C,D).

Table 4
results from thermogravimetric analyses in nitrogen and air for EVA and its compounds.

Atmosphere: nitrogen						
Sample	**T onset [°C]**	**T max 1 [°C]**	**Residue @ T max 1 [%]**	**T max 2 [°C]**	**Residue @ T max 2 [%]**	**Residue @ 800 °C [%]**
EVA	322.5	352.8	91.9	471.6	32.1	0.3
20 BCE-T	325.2	347.7	93.1	471.5	42.0	13.6
40 BCE-T	333.7	354.0	92.8	472.8	51.5	27.1
Atmosphere: air						
Sample	**T onset [°C]**	**T max 1 [°C]**	**Residue @ T max 1 [%]**	**T max 2 [°C]**	**Residue @ T max 2 [%]**	**Residue @ 800 °C [%]**
EVA	304.1	336.9	88.5	431.2	46.9	0.2
20 BCE-T	310.0	338.5	89.4	471.5	29.2	5.8
40 BCE-T	322.3	347.5	91.7	459.1	45.6	15.7

Conversely, the degree of crystallinity (Xc) for all the compounds marginally decreases in the presence of BC, as the filler obstacles the crystallization process of the copolymer, as already reported in the literature [34].

3.6. *Thermogravimetric analyses*

Thermogravimetric analyses were performed in order to evaluate the thermal and thermo-oxidative stability both of BC powder and of its compounds with EVA Fig. 10. shows the thermograms for BC powder in nitrogen and air. In inert atmosphere, BC remains stable until 800 °C with a final residue about 98% of the initial mass. In air, the decomposition occurs in two steps: the first takes place within 350 °C and 570 °C; the second occurs at higher temperatures, i.e. within 630 °C and 700 °C. Beyond 700 °C, BC remains stable, leading to a final residue of about 35% at 800 °C.

Fig. 11 shows the typical TG thermograms for EVA and for its compounds. In nitrogen, EVA shows a two-steps degradation (Table 4 Fig. 11A and B). The first step, occurring between 300 °C and 390 °C, is ascribed to the formation of the acetic acid, where the mass loss is proportional to the quantity of acetate groups initially present in the copolymer. The second decomposition stage (occurring between 405 °C

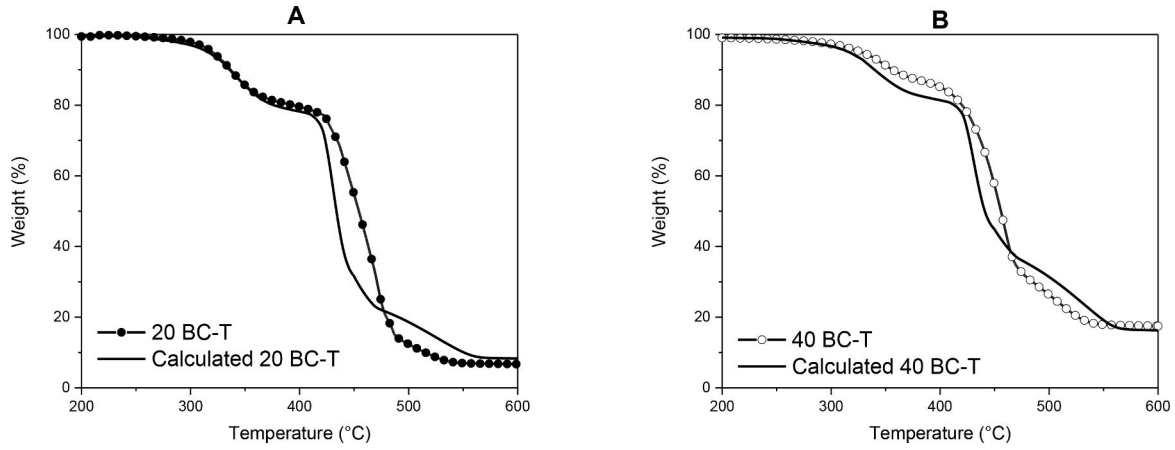

Fig. 12. Comparison between the experimental and calculated TG curves in air for 20 BCE-T and 40 BCE-T compounds.

Table 5
Results from cone calorimetry tests performed on EVA and its compounds.

Specimen	TTI& [s]	pkHRR[kW m^{-2}]	pkHRR Reduction [%]	Time to peak[s]	THR[MJ m^{-2}]	TSR[m^2 m^{-2}]	SEA[m^2 kg^{-1}]	Residue mass[%]	FPI $\left[\frac{(kW/m^2)}{s}\right]$	FIGRA $\left[\frac{(kW/m^2)}{s}\right]$	FRI
EVA	74	1803	–	178	96.6	1280	598	0	24.8	10.1	–
20 BCE-T	44	993	45	142	92.9	1116	442	6	22.6	7.0	1.12
40 BCE-T	43	635	65	105	80.3	1155	527	20	14.8	6.0	1.98
3 BCE-T_sup	112	1405	22	226	111.1	1611	551	1	12.5	6.2	1.69
6 BCE-T_sup	66	1194	34	208	112.5	1739	598	3	18.1	5.7	1.16

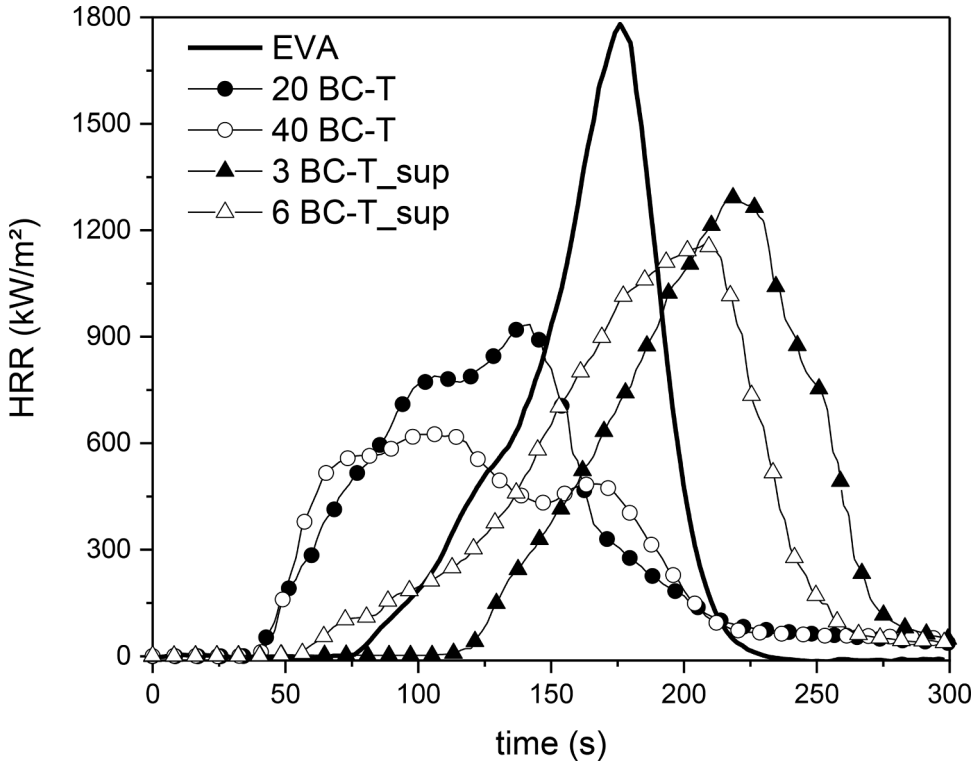

Fig. 13. HRR vs. time cone calorimetry curves of EVA, its bulk compounds and its surface-coated samples.

and 500 °C) is attributable to chain scission phenomena [53]. When the BC is incorporated into EVA, a slight increase of Tonset values, which may be ascribed to a weak protection effect exerted by the filler, is observed, together with a significant increase of the residue at the end of the test.

In air, EVA decomposes according to three consecutive steps (Table 3, Fig. 11C and D). The third decomposition step can be ascribed to the oxidation of the products formed during the previous steps [54].

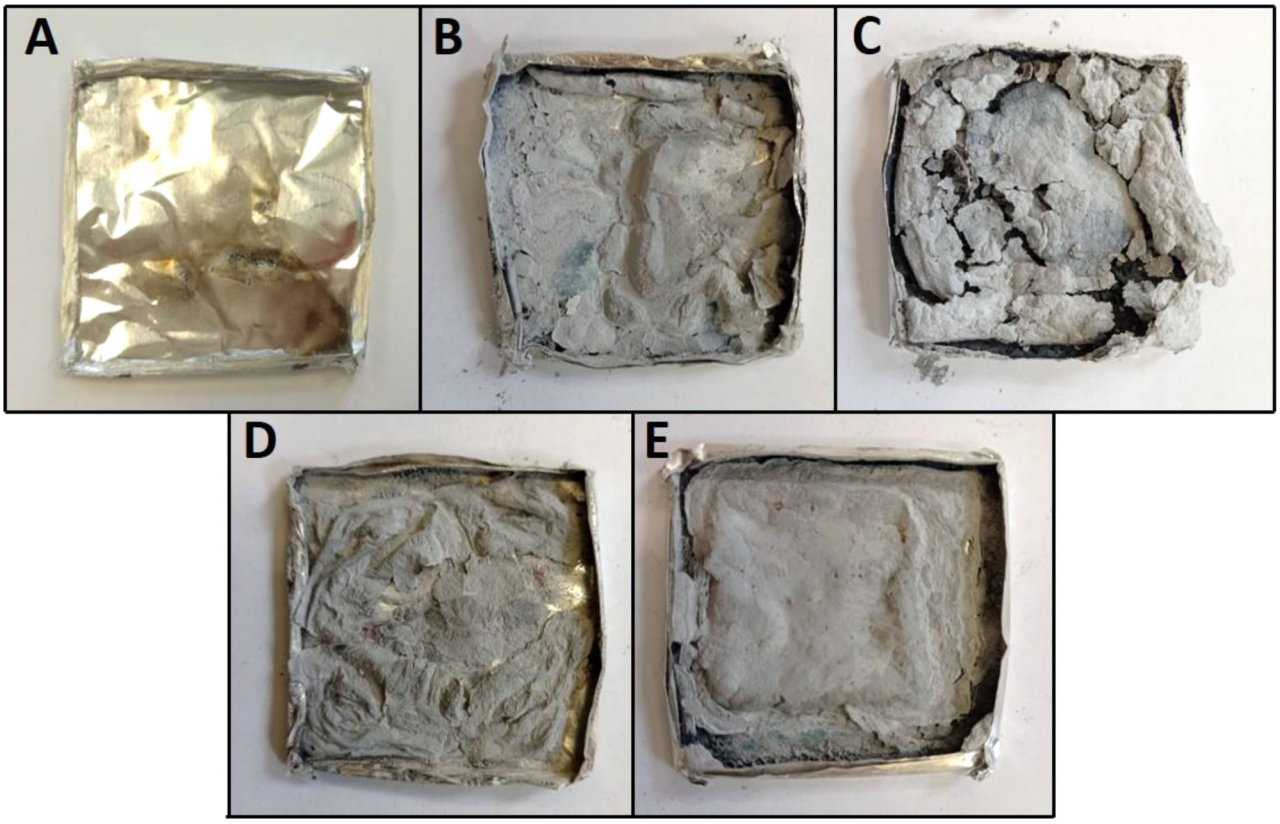

Fig. 14. Residues after cone calorimetry tests of unfilled EVA (A), 20BC-T (B), 40BC-T (C), 3BC-T_sup (D), and 6BC-T_sup (E).

The incorporation of BC at increasing loadings rises Tonset, Tmax1 and Tmax2 values, hence indicating a protection effect exerted by the filler. The highest increase of Tonset and Tmax1 is observed for the highest filler loading (i.e. 40 wt.%), which exhibits temperatures similar to those of unfilled EVA in inert atmosphere. This phenomenon highlights the barrier effect of the filler on oxygen diffusion in the copolymer, as already reported in the literature [55].

In order to evaluate the interactions between EVA and BC particles, the TG curves in air of 20 BCE-T and 40 BCE-T samples were calculated and compared with the corresponding experimental curves (Fig. 12). The experimental 20 BCE-T curve follows the same behavior of the calculated one until the first weight loss step (acetic acid release); the second weight loss step (degradation of unsaturated chains from 405 to 480 °C) occurs at higher temperatures than that observed for the calculated TG curve. This delay is due to the barrier effect exerted by the BC particles. The 40 BCE-T sample seems to show a stronger interaction between polymer matrix and BC, since the experimental curve shows a better thermal stability already from the first degradation step. At higher temperature, the barrier effect toward oxygen is weaker, probably due to the presence of particle aggregates, as observed in SEM micrographs.

3.7. Forced-Combustion behavior

Cone calorimetry tests were performed on EVA and its compounds using a standard irradiative heat flux of 35 kW m − 2. The thermal and smoke parameters recorded during the tests are listed in Table 5; Fig. 13 shows the HRR vs. time curves and Fig. 14 displays the residues at the end of the tests.

From an overall point of view, it is worthy to note that the incorporation of BC remarkably lowers the pkHRR of the samples: this effect is more noticeable increasing the filler loading. In particular, the highest decrease is observed for the samples loaded with 40 wt.% of BC: pkHRR values decrease by about 65% as compared to unfilled EVA. Because of pkHRR decrease, also FPI (pkHRR/TTI ratio) and FIGRA (pkHRR/time to peak) are remarkably lowered in the presence of BC. Besides, the incorporation of BC into the copolymer matrix decreases THR values (by up to 16.9% for the highest BC loading), hence further indicating the protection effect exerted by the filler. In fact, during the combustion, a protective surface layer arising from recession of the polymer from the surface by pyrolysis is created by the accumulation of BC particles left behind. This structure appears to enhance the performance of the char through structural reinforcement acting as thermal and mass transfer barrier, slowing down the escape of volatile products generated during the material decomposition. This finding is supported by the shapes of HRR curves of EVA and its bulk composites (Fig. 13): EVA only shows a single sharp HRR peak, while there are two peaks for its bulk compounds. The occurrence of a single HRR peak can be easily justified, as the sample is gradually burnt. In the second case, the first peak is ascribed to the development of the protective char. After the first peak, the increase in HRR is suppressed due to the presence of the efficient protective barrier. The second peak is likely to be due to the formation of cracks on the protective char previously formed, which weaken the thermal shielding effect exerted by the char layer itself, as the specimen is continuously exposed to the heat [56].

As far as the smoke parameters are considered, the effect of the presence of increasing loadings of BC in the copolymer matrix are quite limited, though a certain decrease of TSR (by about 12.8 and 9.7% for the compounds containing 20 and 40 wt.% of BC, respectively) and SEA (by about 26.1 and 11.9% for the compounds containing 20 and 40 wt.% of BC, respectively) is observed.

Cone calorimetry tests have also been performed on the surface-coated samples. The obtained results are listed in Table 5; Fig. 13 shows the related HRR vs. time curves. By comparing the times to ignition of the samples, the scenario is considerably different between bulk incorporation and surface dispersion of BC. In the first case, the BC filler anticipates both time to ignition and time to peak as compared to

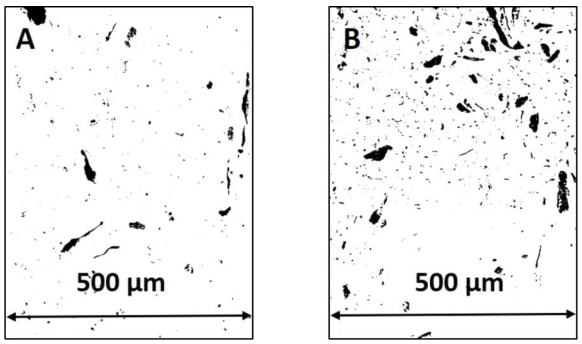

Fig. 15. Detected particles of BC from SEM images of Figs. 8(a) and 8 (b).

unfilled EVA, with similar TTI values for the compounds containing 20 or 40 wt.% of filler, as already reported in literature [34, 57].

Conversely, in the case of samples showing a surface distribution of the filler (i.e. surface-coated specimens), the sample with 3 wt.% of BC surface-distributed is more effective to slow down the ignition (TTI = 112 s) than the counterpart with 6 wt.% of filler (for which, TTI is equal to 66 s), probably because of the better dispersion of the BC particles at the lowest loading. In fact, by increasing the BC loading, the formation of aggregates occurs more frequently. These aggregates act as surface defects, which favor the propagation of cracks within the initial char skin, releasing gasses that facilitate the ignition of the specimen [58]. This assumption was supported by the analysis of the particles distribution on the surface of the coated specimens. A software was used for detecting the BC particles on 3 wt.% and 6 wt.% BC-coated specimens (Fig. 15), and their respective areas were calculated. The results show a total occupied area by the BC of 2.14 and 4.86%, for specimens containing 3 and 6 wt.% of BC, respectively: it is noteworthy that the sample containing 6 wt.% of BC shows bigger and more numerous aggregates, in agreement with the previous hypothesis. However, the effect of an increase of the thermal conductivity of the samples due to the presence of remaining non oxidized metallic particles at the surface cannot be excluded and may further justify the reduction in TTI from 112 to 66 s with increasing the biochar loading.

Both coated-samples show higher time to peak values with respect to unfilled EVA: this finding demonstrates a clear thermal shielding effect provided by the presence of the filler on the surface of the sample exposed to the irradiative heat flux. It is further noteworthy that all the compounds, despite the strategy adopted for conferring flame retardance to EVA (i.e., bulk or surface approach), show Flame Retardancy Index values within 1 and 10, hence being classified as "good" [45].

Besides, as far as the surface-coated samples are considered, the appearance of cracks during the forced-combustion tests on the surface exposed to the irradiative heat flux limits the protection capability exerted on the underlying unfilled copolymer, hence further supporting the better performances observed for the bulk compounds.

3.8. *Temperature profiles during forced-combustion tests*

In order to assess the potential thermal shielding effect provided by the filler, the temperature profiles during combustion were recorded on the surface and on the backside of the samples of EVA and its compounds Fig. 16. shows the temperature profiles of the tested samples: the temperature profile on the surface directly exposed to the irradiative heat flux is displayed by the curve named as T surface, while the other curves show the temperature trends measured on the backside of the different specimens. As shown in Fig. 16, the temperature measured on the surface increases rapidly due to its proximity to the cone heater, reaching about 600 °C at the end of the forced-combustion test. The presence of BC reveals its thermal shielding effect, lowering the temperatures

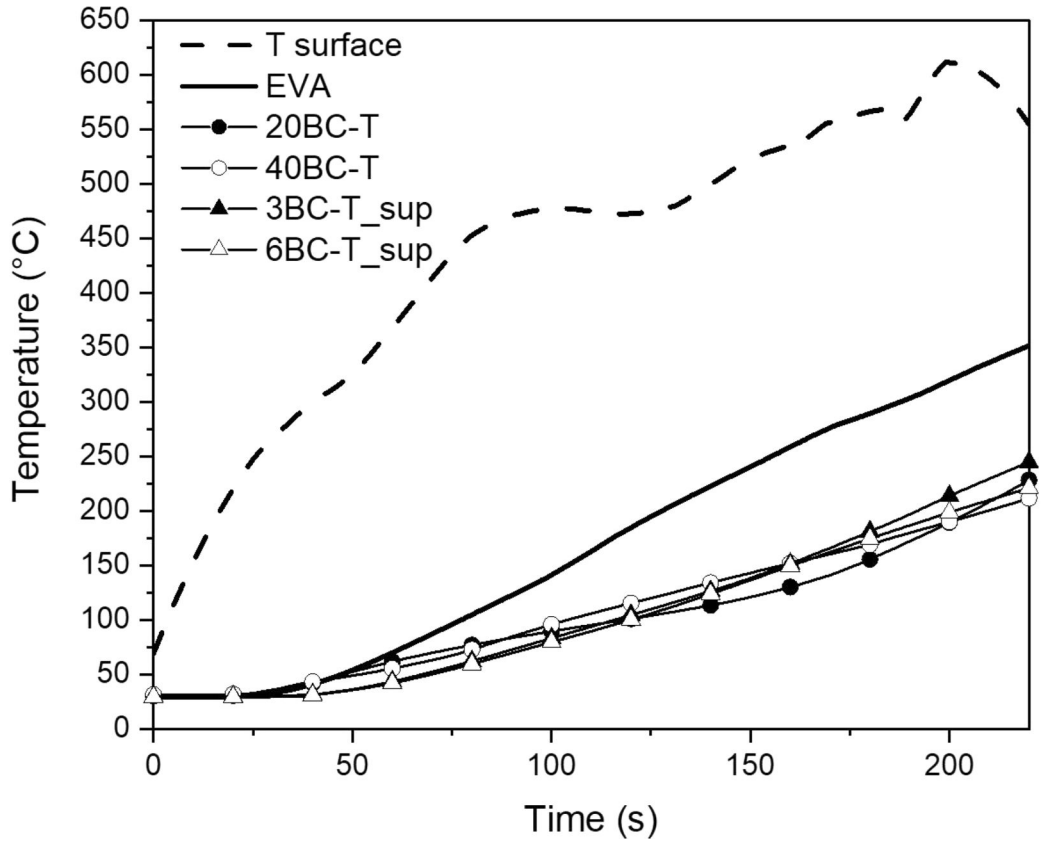

Fig. 16. Temperature profiles recorded on the surface (dotted line) exposed to the irradiative heat flux (35 kW $m-2$) and on the backside of the samples during forced-combustion tests.

recorded on the specimen backside. More specifically, the temperatures detected by the thermocouple placed on the back of the specimens containing BC are about 100–140 °C lower as compared to unfilled EVA, irrespective of the type of specimen (i.e. bulk or surface-coated sample) and BC loading. These findings indicate the possibility to minimize the quantity of biochar employed (i.e. from 40 wt.% in bulk to 3 wt.% in surface) to achieve the same thermal shielding performances.

4. Conclusions

In this work, the pyrolytic conversion of Tetra Pak® for the production of alumina-rich biochar was reported. The obtained BC was incorporated into bulk EVA through compounding or applied to unfilled EVA matrix as a surface coating, and its use as flame retardant was thoroughly investigated. The BC loadings selected were 20 and 40 wt.% for bulk incorporation and 3 and 6 wt.% for the surface coating. XPS analysis clearly showed that the alumina represents the greatest part of aluminum species (reaching 74%) and the massive presence of sp2 carbon leads to the formation of quite ordered carbonaceous materials, as further confirmed by Raman spectroscopy. SEM-EDX images of compounds highlighted a good distribution of BC within the polymer matrix, with micrometric dispersion of the particles not exceeding 100 μm. DSC analysis shows a marginally decrease of the degree of crystallinity for all the compounds in the presence of BC, with respect to unfilled EVA. Conversely, the thermal and thermo-oxidative stability of compounds were enhanced, hence indicating a protection effect exerted by the BC filler. Cone calorimetry tests were exploited for assessing the combustion behavior of the designed compounds. In this context, the bulk approach promoted a remarkable decrease of peak of heat release rate (up to 65%) and of total heat release (up to 17%), combined with a significant increase of the residues at the end of the tests, with respect to unfilled EVA. Conversely, the surface approach was only capable to delay the time to ignition (+38 s) and the time to peak of HRR (+48 s), depending of the BC loading. In addition, the profile temperatures of the specimens were recorded, revealing a thermal shielding effect exerted by the BC particles.

Finally, despite the overall improvement of the fire retardance, the incorporation of BC negatively affected the ductility of EVA, making the copolymer, at the same time, stiffer.

Data availability

The raw data required to reproduce these findings are available upon request.

Declaration of Competing Interests

The authors declare that they have no known competing financial interests or personal relationships that could have appeared to influence the work reported in this paper.

References

[1] J. Rybicka, A. Tiwari, G.A. Leeke, Technology readiness level assessment of composites recycling technologies, J. Clean. Prod 112 (2016) 1001–1012.
[2] Tetrapak, Go Nature, Go Carton (2020).
[3] H. Jones, Tetra pak—A model for successful innovation, Long Range Plann 15 (6) (1982) 31–37.
[4] E. Chiellini, A. Barghini, P. Cinelli, V. Ilieva, Overview of environmentally compatible polymeric materials for food packaging, Environmentally Compatible Food Packaging: Elsevier (2008) 371–395.
[5] J. Zawadiak, S. Wojciechowski, T. Piotrowski, A. Krypa, Tetra pak recycling—current trends and new developments, Am. J. Chem. Eng. 5 (3) (2017) 37–42.
[6] D. Foti, S. Adamopoulos, E. Voulgaridou, E. Voulgaridis, C. Passialis, S. O. Amiandamhen, et al., Microstructure and compressive strength of gypsum-bonded composites with papers, paperboards and Tetra Pak recycled materials, J. Wood Sci 65 (1) (2019) 1–8.
[7] Martínez-Barrera G., Barrera-Díaz C.E., Cuevas-Yañez E., Varela-Guerrero V., Vigueras-Santiago E., Ávila-Córdoba L., et al. Waste cellulose from Tetra Pak packages as reinforcement of cement concrete. Advances in materials science and engineering. 2015;2015.
[8] O. Platnieks, A. Barkane, N. Ijudina, G. Gaidukova, V.K. Thakur, S. Gaidukovs, Sustainable tetra pak recycled cellulose/Poly (Butylene succinate) based woody-like composites for a circular economy, J. Clean. Prod 270 (2020), 122321.
[9] M. Karaboyaci, Process design for the recycling of tetra Pak components, Eur. J. Eng. Nat. Sci 2 (1) (2017) 126–129.
[10] J.-F. Zhang, Yan d-h, Li Z-h, The recycling of the Tetra-Pak packages: research on the wet process separation conditions of aluminum and polythene in the Tetra-Pak packages, 2009 3rd Int. Conf. Bioinform. Biomed. Eng.: IEEE (2009) 1–6.
[11] L. Xing, J. Gu, W. Zhang, D. Tu, C Hu, Cellulose I and II nanocrystals produced by sulfuric acid hydrolysis of Tetra pak cellulose I, Carbohydr. Polym 192 (2018) 184–192.
[12] C.I.K. Diop, J.-.M. Lavoie, Isolation of nanocrystalline cellulose: a technological route for valorizing recycled tetra pak aseptic multilayered food packaging wastes, Waste Biomass Valorization 8 (1) (2017) 41–56.
[13] A. Undri, L. Rosi, M. Frediani, P. Frediani, Fuel from microwave assisted pyrolysis of waste multilayer packaging beverage, Fuel 133 (2014) 7–16.
[14] J. Haydary, D. Susa, J. Dudáš, Pyrolysis of aseptic packages (tetrapak) in a laboratory screw type reactor and secondary thermal/catalytic tar decomposition, Waste Manage. (Oxford) 33 (5) (2013) 1136–1141.
[15] A. Korkmaz, J. Yanik, M. Brebu, C. Vasile, Pyrolysis of the tetra pak, Waste Manage. (Oxford) 29 (11) (2009) 2836–2841.
[16] K. Tekin, S. Ucar, S. Karagöz, Influence of co-pyrolysis of waste tetra pak with waste motor oil on product distribution and properties for fuel application, Energy Fuels 33 (11) (2019) 11101–11112.
[17] J.S. Cha, S.H. Park, S.-.C. Jung, C. Ryu, J.-.K. Jeon, M.-.C. Shin, et al., Production and utilization of biochar: a review, J. Ind. Eng. Chem. 40 (2016) 1–15.
[18] S.P. Sohi, E. Krull, E. Lopez-Capel, R. Bol, A review of biochar and its use and function in soil, Adv. Agron.: Elsevier (2010) 47–82.
[19] M. Ahmad, A.U. Rajapaksha, J.E. Lim, M. Zhang, N. Bolan, D. Mohan, et al., Biochar as a sorbent for contaminant management in soil and water: a review, Chemosphere 99 (2014) 19–33.
[20] M. Bartoli, M. Giorcelli, P. Jagdale, M. Rovere, A Tagliaferro, A Review of Non-Soil Biochar Applications. Materials. 13 (2) (2020) 291–296.
[21] B. Zuccarello, M. Bartoli, F. Bongiorno, C. Militello, A. Tagliaferro, A. Pantano, New concept in bioderived composites: biochar as toughening agent for improving performances and durability of agave-based epoxy biocomposites, Polymers (Basel) 13 (2) (2021) 198.
[22] D. Torsello, G. Ghigo, M. Giorcelli, M. Bartoli, M. Rovere, A. Tagliaferro, Tuning the microwave electromagnetic properties of biochar-based composites by annealing, Carbon Trends (2021), 100062.
[23] M. Giorcelli, M. Bartoli, A. Sanginario, E. Padovano, C. Rosso, M. Rovere, et al., High-temperature annealed biochar as a conductive filler for the production of piezoresistive materials for energy conversion application, ACS Appl. Electron. Mater. 3 (2) (2021) 838–844.
[24] V. Strongone, M. Bartoli, P. Jagdale, R. Arrigo, A. Tagliaferro, G. Malucelli, Preparation and characterization of UV-LED curable acrylic films containing biochar and/or multiwalled carbon nanotubes: effect of the filler loading on the rheological, thermal and optical properties, Polymers (Basel) 12 (4) (2020).
[25] P. Savi, M. Yasir, M. Bartoli, M. Giorcelli, M. Longo, Electrical and microwave characterization of thermal annealed sewage sludge derived biochar composites, Applied Sciences 10 (4) (2020) 1334–1345.
[26] A. Noori, M. Bartoli, A. Frache, E. Piatti, M. Giorcelli, A. Tagliaferro, Development of pressure-responsive polypropylene and biochar-based materials, Micromachines (Basel) 11 (4) (2020) 339.
[27] R. Arrigo, M. Bartoli, Malucelli G. Poly, (lactic Acid)–Biochar biocomposites: effect of processing and filler content on rheological, Thermal, and Mechanical Properties. Polymers 12 (4) (2020) 892.
[28] M. Bartoli, M. Giorcelli, C. Rosso, M. Rovere, P. Jagdale, A Tagliaferro, Influence of commercial biochar fillers on brittleness/ductility of epoxy resin composites, Appl. Sci. 9 (15) (2019) 13.
[29] W. Jerzak, A. Bieniek, A. Magdziarz, Multifaceted analysis of products from the intermediate co-pyrolysis of biomass with Tetra Pak waste, Int. J. Hydrogen Energy (2021) in press.
[30] H. Huo, Y. Ma, X. Wang, Recovery of aluminum and preparation of porous carbon from Tetra Pak waste, ChemistrySelect 6 (8) (2021) 1814–1822.
[31] M. Muñoz-Batista, G. Blázquez, J. Franco, M. Calero, M. Martín-Lara, Recovery, separation and production of fuel, plastic and aluminum from the Tetra PAK waste to hydrothermal and pyrolysis processes, Waste Manage. (Oxford) 137 (2022) 179–189.
[32] Z. Ding, X. Xu, T. Phan, X. Hu, G. Nie, High adsorption performance for As (III) and As (V) onto novel aluminum-enriched biochar derived from abandoned Tetra Paks, Chemosphere 208 (2018) 800–807.
[33] N.M. Zúñiga-Muro, A. Bonilla-Petriciolet, D.I. Mendoza-Castillo, C.J. Duran-Valle, J. Silvestre-Albero, H.E. Reynel-Avila, et al., Recycling of Tetra pak wastes via pyrolysis: characterization of solid products and application of the resulting char in the adsorption of mercury from water, J. Clean. Prod 291 (2021), 125219.
[34] S. Matta, M. Bartoli, A. Frache, G. Malucelli, Investigation of different types of biochar on the thermal stability and fire retardance of ethylene-vinyl acetate copolymers, Polymers (Basel) 13 (8) (2021) 1256.
[35] M. Barbalini, M. Bartoli, A. Tagliaferro, G. Malucelli, Phytic acid and biochar: an effective all bio-sourced flame retardant formulation for cotton fabrics, Polymers (Basel) 12 (4) (2020) 811.
[36] F. Cravero, A. Frache, Improving fire performances of PEAL: more second-life options for recycled Tetra Pak®, Polymers (Basel) 12 (10) (2020) 2357.

[37] H. Raclavská, J. Růžičková, H. Škrobánková, S. Koval, M. Kucbel, K. Raclavský, et al., Possibilities of the utilization of char from the pyrolysis of tetrapak, J. Environ. Manage. 219 (2018) 231–238.
[38] O. Das, N.K. Kim, A.L. Kalamkarov, A.K. Sarmah, D. Bhattacharyya, Biochar to the rescue: balancing the fire performance and mechanical properties of polypropylene composites, Polym. Degrad. Stab. 144 (2017) 485–496.
[39] Q. Zhang, H. Cai, K. Yang, W Yi, Effect of biochar on mechanical and flame retardant properties of wood–plastic composites, Results in Physics 7 (2017) 2391–2395.
[40] O. Das, D. Bhattacharyya, D. Hui, K.-.T. Lau, Mechanical and flammability characterisations of biochar/polypropylene biocomposites, Compos. B. Eng. 106 (2016) 120–128.
[41] S.T. Lazar, T.J. Kolibaba, J.C. Grunlan, Flame-retardant surface treatments, Nat. Rev. Mater. 5 (4) (2020) 259–275.
[42] J. Alongi, A. Di Blasio, F. Cuttica, F. Carosio, G. Malucelli, Bulk or surface treatments of ethylene vinyl acetate copolymers with DNA: investigation on the flame retardant properties, Eur. Polym. J 51 (2014) 112–119.
[43] D. Battegazzore, J. Alongi, G. Fontaine, A. Frache, S. Bourbigot, G. Malucelli, Bulk vs. surface flame retardancy of fully bio-based polyamide 10, 10, RSC Adv 5 (49) (2015) 39424–39432.
[44] A. Tagliaferro, M. Rovere, E. Padovano, M. Bartoli, M. Giorcelli, Introducing the Novel Mixed Gaussian-Lorentzian Lineshape in the Analysis of the Raman Signal of Biochar, Nanomaterials. 10 (9) (2020) 1748.
[45] H. Vahabi, B.K. Kandola, M.R. Saeb, Flame retardancy index for thermoplastic composites, Polymers (Basel) 11 (3) (2019) 407.
[46] Y.-.C. Lin, J. Cho, G.A. Tompsett, P.R. Westmoreland, G.W. Huber, Kinetics and mechanism of cellulose pyrolysis, J. Phys. Chem. C 113 (46) (2009) 20097–20107.
[47] S. Wang, Q. Liu, Y. Liao, Z. Luo, K. Cen, A study on the mechanism research on cellulose pyrolysis under catalysis of metallic salts, Korean J. Chem. Eng. 24 (2) (2007) 336–340.
[48] N.D. Parkyns, The surface properties of metal oxides. Part II. An infrared study of the adsorption of carbon dioxide on γ-alumina, J. Chem. Soc. A (0) (1969) 410–417.
[49] P.M. Sherwood, Introduction to studies of aluminum and its compounds by XPS, Surf. Sci. Spectra 5 (1) (1998) 1–3.
[50] C.J. Biermann, Handbook of Pulping and Papermaking, Academic Press, San Diego, U.S., 1996.
[51] G. Camino, A. Maffezzoli, M. Braglia, M. De Lazzaro, M. Zammarano, Effect of hydroxides and hydroxycarbonate structure on fire retardant effectiveness and mechanical properties in ethylene-vinyl acetate copolymer, Polym. Degrad. Stab. 74 (3) (2001) 457–464.
[52] S. Bourbigot, M. Le Bras, S. Duquesne, M Rochery, Recent advances for intumescent polymers, Macromol. Mater. Eng 289 (6) (2004) 499–511.
[53] M. Marin, A. Jiménez, J. López, J. Vilaplana, Thermal degradation of ethylene (vinyl acetate) Kinetic analysis of thermogravimetric data, J. Therm. Anal. Calorim. 47 (1) (1996) 247–258.
[54] B. Rimez, H. Rahier, G. Van Assche, T. Artoos, M. Biesemans, B. Van Mele, The thermal degradation of poly (vinyl acetate) and poly (ethylene-co-vinyl acetate), Part I: experimental study of the degradation mechanism, Polym. Degrad. Stab. 93 (4) (2008) 800–810.
[55] A. Fina, H. Abbenhuis, D. Tabuani, A. Frache, G. Camino, Polypropylene metal functionalised POSS nanocomposites: a study by thermogravimetric analysis, Polym. Degrad. Stab. 91 (5) (2006) 1064–1070.
[56] X. Wu, L. Wang, C. Wu, J. Yu, L. Xie, G. Wang, et al., Influence of char residues on flammability of EVA/EG, EVA/NG and EVA/GO composites, Polym. Degrad. Stab. 97 (1) (2012) 54–63.
[57] S. Bourbigot, J. Sarazin, F. Samyn, M. Jimenez, Intumescent ethylene-vinyl acetate copolymer: reaction to fire and mechanistic aspects, Polym. Degrad. Stab. 161 (2019) 235–244.
[58] A. Fina, G Camino, Ignition mechanisms in polymers and polymer nanocomposites, Polym. Adv. Technol 22 (7) (2011) 1147–1155.